J|A|C|S
ARTICLES
Published on Web 05/19/2006

Kinetics of RNA Refolding in Dynamic Equilibrium by ^{1}H-Detected ^{15}N Exchange NMR Spectroscopy

Philipp Wenter,[†] Geoffrey Bodenhausen,[†,‡] Jens Dittmer,*[,§] and Stefan Pitsch*[,†]

Contribution from the Institute of Chemical Sciences and Engineering, Ecole Polytechnique Fédérale de Lausanne, EPFL, Batochime, 1015 Lausanne, Switzerland, Département de Chimie, associé au CNRS, Ecole Normale Supérieure, 24 Rue Lhomond, 75231 Paris Cedex 05, France, and Kemisk Institut, Aarhus Universitet, Langelandsgade 140, 8000 Aarhus C, Denmark

Received January 17, 2006; E-mail: dittmer@chem.au.dk; stefan.pitsch@epfl.ch

Abstract: By implementing new NMR methods that were designed to map very slow exchange processes we have investigated and characterized the refolding kinetics of a thermodynamically stable 34mer RNA sequence in dynamic equilibrium. The RNA sequence was designed to undergo a topologically favored conformational exchange between different hairpin folds, serving as a model to estimate the minimal time required for more complex RNA folding processes. Chemically prepared RNA sequences with sequence-selective ^{15}N labels provided the required signal separation and allowed a straightforward signal assignment of the imino protons by HNN correlation experiments. The 2D version of the new ^{1}H-detected ^{15}N exchange spectroscopy (EXSY) pulse sequence provided cross-peaks for resonances belonging to different folds that interchange on the time scale of longitudinal relaxation of ^{15}N nuclei bound to imino protons. The 34mer RNA sequence exhibits two folds which exchange on the observable time scale ($\tau_{obs} \approx T_1\{^{15}N\} <$ 5 s) and a third fold which is static on this time scale. A 1D version of the ^{15}N exchange experiment allowed the measurement of the exchange rates between the two exchanging folds as a function of temperature and the determination of the corresponding activation energies E_a and frequency factors A. We found that the refolding rates are strongly affected by an entropically favorable preorientation of the replacing strand. The activation energies are comparable to values obtained for the slow refolding of RNA sequences of similar thermodynamic stability but less favorable topology.

1. Introduction

RNA sequences can adopt different coexisting folds on the level of secondary and/or tertiary structure.[1] The underlying folding and refolding processes cover a wide temporal range. Typically, folding from an unfolded state is observed on a time scale of $\tau = 10^{-5} - 1$ s,[2] whereas secondary structure refolding and tertiary structure reorganization can occur within $\tau = 1 - 10^{4}$ s.[3] A full characterization of RNA requires not only the determination of its structure, but also a description of its folding dynamics and pathways.[4,5] Time-resolved RNA folding and refolding from a nonequilibrium state has been investigated by native gel electrophoresis,[6] chemical[4,7] and enzymatic[8] footprinting, UV,[9,10] fluorescence,[11] and NMR[10,12] spectroscopy. So far, no RNA folding study in an unperturbed dynamic equilibrium has been reported, mainly due to the lack of suitable methods. In principle, structural fluctuations in equilibrium can be directly observed either by fluorescence correlation spectroscopy or by NMR spectroscopy, which provides detailed information about the associated structural changes, at least for smaller systems. For the characterization of internal dynamics of proteins, a variety of NMR experiments are employed; processes on a time scale $\tau = 10^{-10} - 10^{-2}$ s are analyzed by line shape and relaxation measurements, and processes on a time scale $\tau = 10^{-2} - 1$ s by exchange-sensitive experiments.

An inspection of the ribosome structure by Noller[13] has revealed that almost all base paired regions contain seven or

[†] Ecole Polytechnique Fédérale.
[‡] Ecole Normale Supérieure.
[§] Aarhus Universitet.

(1) (a) Brion, P.; Westhof, E. *Annu. Rev. Biophys. Biomol. Struct.* **1997**, *26*, 113−137. (b) Huthoff, H.; Berkhout, B. *Nucleic Acids Res.* **2001**, *29*, 2594−2600. (c) Höbartner, C.; Micura, R. *J. Mol. Biol.* **2003**, *325*, 421−431.
(2) Woodson, S. A. *Cell. Mol. Life Sci.* **2000**, *57*, 796−808.
(3) (a) Treiber, D. K.; Rook, M. S.; Zarrinkar, P. P.; Williamson, J. R. *Science* **1998**, *279*, 1943- 1946. (b) Pan, J.; Thirumalai, D.; Woodson, S. A. *J. Mol. Biol.* **1997**, *273*, 7−13.
(4) Chaulk, S. G.; MacMillan, A. M. *Biochemistry* **2000**, *39*, 2−8.
(5) Zarrinkar, P. P.; Wang, J.; Williamson, J. R. *RNA* **1996**, *2*, 564−573.
(6) Gluick, T. C.; Gerstner, R. B.; Draper, D. E. *J. Mol. Biol.* **1997**, *270*, 451−463.
(7) Sclavi, B.; Sullivan, M.; Chance, M. R.; Brenowitz, M.; Woodson, S. A. *Science* **1998**, *279*, 1940−1943.
(8) Zarrinkar, P. P.; Williamson, J. R. *Science* **1994**, *265*, 918−924.
(9) (a) LeCuyer, K. A.; Crothers, D. M. *Proc. Natl. Acad. Sci. U.S.A.* **1994**, *91*, 3373−3377. (b) Nagel, J. H. A.; Gultyaev, A. P.; Öistämö, K. J.; Gerdes, K.; Pleij, C. W. A. *Nucleic Acids Res.* **2002**, *30*, e63. (c) Hamori, E.; Iio, T.; Senior, M. B.; Gutierrez, P. L. *Biochemistry* **1975**, *14*, 3618−3625; (d) Cole, P. E.; Crothers, D. M. *Biochemistry* **1972**, *11*, 4368−4374. (e) Coutts, S. M. *Biochim. Biophys. Acta* **1971**, *232*, 94−106. (f) Pörschke, D. *Mol. Biol. Biochem. Biophys.* **1977**, *24*, 191−218.
(10) Bina-Stein, M.; Crothers, D. M. *Biochemistry* **1975**, *14*, 4185−4191.
(11) (a) Walter, N. G.; Harris, D. A.; Pereira, M. J. B.; Rueda, D. *Biopolymers* **2002**, *61*, 224−241; (b) Ha, T.; Zhuang, X.; Kim, H. D.; Orr, J. W.; Williamson, J. R.; Chu, S. *Proc. Natl. Acad. Sci. U.S.A.* **1999**, *96*, 9077−9082. (c) Lynch, D. C.; Schimmel, P. R. *Biochemistry* **1974**, *13*, 1841-1852.
(12) (a) Wenter, P.; Fürtig, B.; Hainard, A.; Schwalbe, H.; Pitsch, S. *Angew. Chem., Int. Ed.* **2005**, *44*, 2600−2603. (b) Wenter, P.; Fürtig, B.; Hainard, A.; Schwalbe, H.; Pitsch, S. *ChemBioChem* **2006**, *407*, 417−420.
(13) Noller, H. F. *Science* **2005**, *309*, 1508−1514.

fewer contiguous Watson−Crick base pairs. To characterize the dynamics of such naturally occurring RNA substructures, we recently determined the refolding kinetics of two representative bistable 20mer RNA sequences, each switching between two alternative, thermodynamically stable hairpin structures composed of 4−6 base pair stems ($\Delta H = 50-60$ kcal mol^{-1}). These experiments were carried out by a combination of photoinduced release of caged RNAs and real-time NMR experiments. We found that the refolding processes of these very small bistable model sequences are surprisingly slow, occurring with $\tau \approx 5-100$ s at 283−298 K.[12] Stimulated by this result, we attempted to estimate the upper range for refolding rates of secondary RNA structures and to investigate the relation between structural features and kinetic parameters of refolding. Here, we report these parameters for a representative 34mer RNA sequence, which was designed to undergo a relatively fast strand replacement between coexisting folds in the time range accessible by exchange-sensitive NMR spectroscopy (EXSY). The exchange rates were obtained by new 1D and 2D ^{1}H/^{15}N-heteronuclear exchange-sensitive NMR methods, which exploit the long longitudinal relaxation times $T_1\{^{15}N\}$ and separate the effect of structural exchange (refolding) from the interfering effects of water exchange.

2. Results

2.1. Sequence Design and Structural Assignment. We designed RNA sequences that can switch between two alternative hairpin folds, each with a representative stem of eight base pairs. The common element in both folds is one of the stem-forming strands. Two alternative partner strands are competing for base pair formation with this common target strand and two stable GCGA tetraloops connect the target and the two alternative partner strands. An unambiguous distinction of the two possible folds by imino proton spectroscopy was achieved by introducing a C and a U, respectively, in the two competing strands, as alternative pairing partners for the same G of the target strand. In addition, the N(1) of this guanosine was ^{15}N-labeled (= ^{15N}G) to enable a straightforward structural probing by ^{15}N-filtered imino proton spectroscopy.[14]

Following these design rules, we prepared a series of RNA sequences and analyzed them by NMR for the coexistence of two alternative folds. The 34mer RNA sequence 5′-r[CACUUGAGGCGACUCA(^{15N}G)GUGAGGCGACUCACCUG]-3′ showed two distinct signals in the ^{15}N−HSQC spectrum (3:2 ratio at 293 K) and was therefore selected for this study (Figure 1b). The chemical shifts at 12.7 and 10.7 ppm are typical for the presence of G:C and G:U base pairs, respectively. The imino proton NMR spectrum of this RNA sequence shows a large number of strongly overlapping signals, consistent with the coexistence of several folds (Figure 1a). This severe signal overlap prevented a detailed secondary structure analysis by conventional ^{1}H NOESY spectroscopy. However, assignments could be obtained by HNN correlation experiments, which correlate the H-bond donor and the H-bond acceptor nitrogen nuclei within a base pair.[15] A set of four sequences with selectively ^{15}N-labeled nucleotides at different positions was prepared, providing a confirmation of the expected base pairing. In Figure 2a−d, the corresponding HNN correlation spectra are

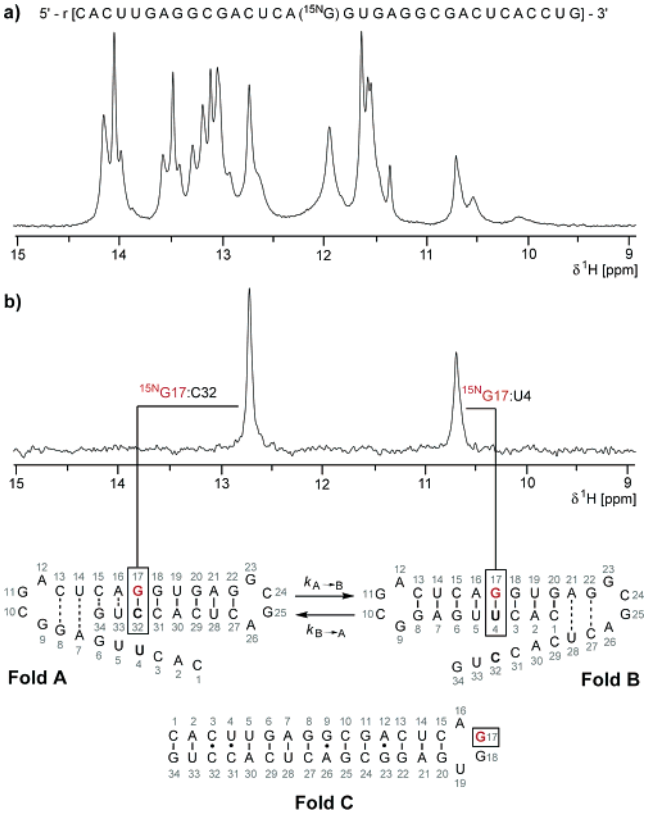

Figure 1. Imino proton signals of the 34mer RNA sequence (0.5 mM) containing a ^{15}N(1)-labeled guanosine at position 17 (^{15N}G17), recorded at 293 K. (a) ^{15}N-decoupled 1D ^{1}H NMR spectrum. (b) ^{15}N-filtered ^{1}H spectrum, showing signals for each base pair formed by ^{15N}G17 and their assignment to folds A and B, respectively, according to the experiments shown in Figure 2. In fold C, ^{15N}G17 is not forming any base pair so that its imino proton exchanges too rapidly with the solvent to be detected.

shown, which allowed a straightforward detection and assignment of the indicated base pairs and corroborated the presence of the two folds A and B. Furthermore, these experiments revealed the presence of a third fold C, which was not detected in Figure 1b. Its extended hairpin structure, with a large number of base pair mismatches is shown in Figures 1 and 2. It was determined by subsequent HNN correlation experiments of a second set of four differently ^{15}N-labeled sequences, which provided an assignment of the base pairs (Figure 2e,f) and excluded an alternative, self-complementary duplex structure (Supporting Information Figure S1).

Whereas all base pairs in fold B could be confirmed by the presence of two HNN correlation cross-peaks (Figure 2c,d), such signals were absent for the two outermost base pairs C15:G34 and A16:U33 of fold A and only a very weak signal for the U33 and G34 imino protons could be detected in the 1D ^{15}N-filtered ^{1}H spectrum (Figure 2b). The signals of the outermost base pairs C1:G20 and A2:U19 of fold B are attenuated to a lesser extent. Indeed, in fold B there is an additional stabilizing stacking interaction between the last G20:C1 base pair and the 3′-adjacent A21 overhang, rendering it more rigid than the analogous G34:C15 base pair in fold A, which lacks a similar stabilizing interaction. In the absence of a stabilizing 3′-overhang, the imino proton signals of the two last base pairs in fold A are strongly attenuated by fast water exchange and therefore undetectable in HNN correlation experiments.

2.2. Thermodynamics and Water Exchange Studies. The ^{15}N-filtered imino proton spectra revealed that the relative signal

(14) Wenter, P.; Pitsch, S. *Helv. Chim. Acta* **2003**, *86*, 3955−3974.
(15) Dingley, A. J.; Grzesiek, S. *J. Am. Chem. Soc.* **1998**, *120*, 8293−8297.

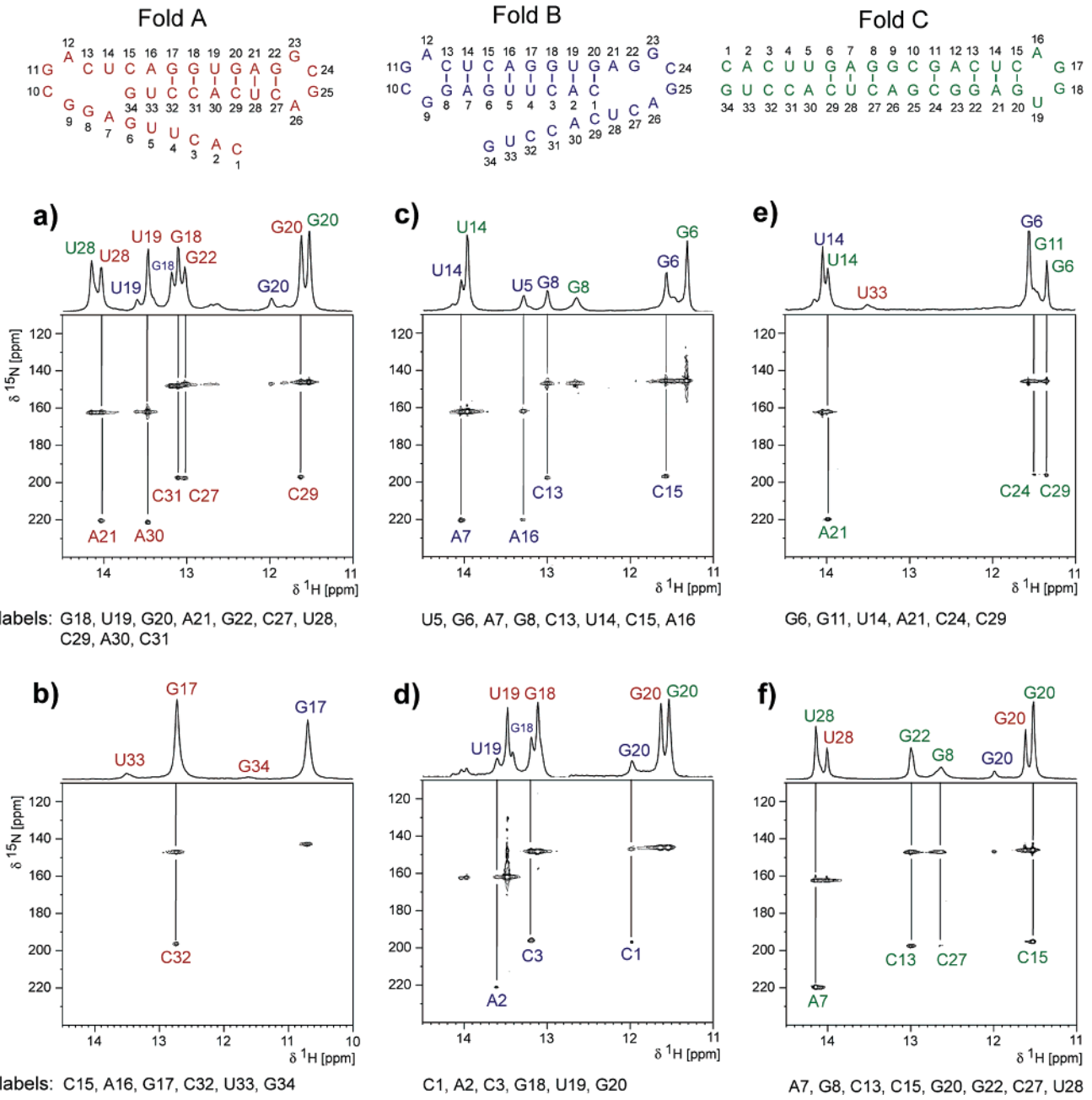

Figure 2. Unambiguous assignment of the three folding structures A, B, and C by separate detection of all indicated base pairs in HNN correlation experiments;[15] in fold A, the terminal base pairs G34:C15 and U33:A16 are too dynamic to be detected. a−f): 1D ^{15}N-filtered ^{1}H spectra and HNN correlation spectra of the 34mer RNA sequence (0.5−0.8 mM) containing six different combinations of ^{15}N-labeled donor and acceptor nucleotides at the indicated positions, recorded at 293 K; each of the ^{15}N-labeled donor nucleotides (^{15}N(1)-guanosines and ^{15}N(3)-uridines) shows a signal in the 1D spectrum and one ^{1}H−^{15}N cross-peak. An additional ^{1}H−^{15}N cross-peak from acceptor nucleotides (^{15}N(1)-adenosines and ^{15}N(3)-cytidines) appears only if both nucleotides of a base pair are ^{15}N-labeled, as indicated by vertical lines in the spectra. The color code relates these detected base pairs to the three folds A, B, and C.

intensities of the three different folds A, B, and C were strongly temperature-dependent and varied from approximately 3:3:4 at 283 K to 7:1:2 at 303 K. At higher temperatures, only signals for fold A could be observed (Supporting Information Figure S2). The low thermal stability of fold C was also detected by temperature-dependent UV spectroscopy, in which the corresponding transition is observed around 300 K (Figure 3a). In the following thermodynamic and kinetic analyses fold C will be neglected, as it appears static on the NMR time scale (see Figure 5). To study the exchange between folds A and B, we have selected the ^{15}N−G17 singly labeled sequence from Figure 1. Its ^{15}N-edited ^{1}H spectrum shows only the well-separated imino proton signals of the base pairs G17:U4 and G17:C32 for folds A and B and no signal for the unpaired G17 in fold C (see Figure 1b).

For the determination of the relative concentrations of folds A and B from ^{15}N-filtered imino proton spectra, we had to account for the different signal attenuation during INEPT transfers due to the different water exchange rates of the G17:U4 and G17:C32 base pairs that are not equally accessible to solvent exchange. This was achieved by weighting the fitted and integrated signal intensities by a factor $\exp\{-4\tau\, k_{H2O}\}$ for the two INEPT steps. The temperature-dependent water exchange rates k_{H2O} were determined independently by selective

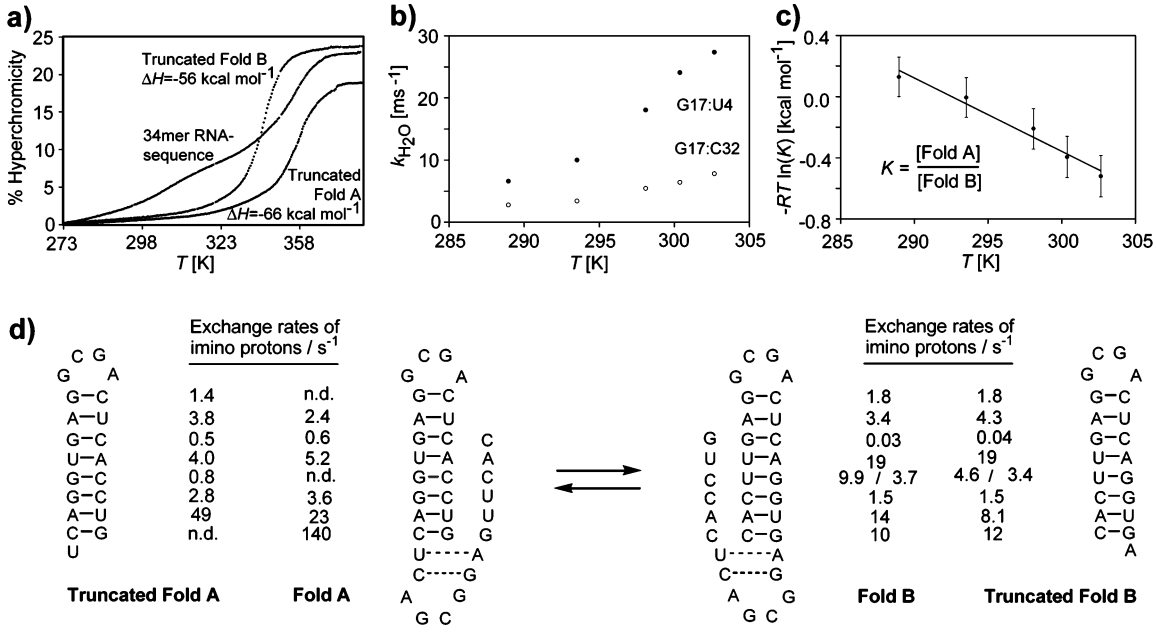

Figure 3. (a) Thermal denaturation curves of the 34mer RNA sequence and the two truncated 21mer hairpins, representative of folds A and B (structures in Figure 3d), as obtained by UV spectroscopy at 260 nm (5 μM in the NMR buffer); the indicated enthalpies of hairpin formation ΔH were determined according to an established procedure;[17] for the low-temperature transition of fold C at 300 K a $\Delta H \approx -40$ kcal mol^{-1} has been determined. (b) Temperature-dependent exchange rates of imino protons with solvent water in ^{15N}G17:U4 (fold B) and ^{15N}G17:C32 (fold A). (c) Linearized plot of the temperature dependence of the equilibrium constant $K =$ [fold A]/[fold B] according to $-RT\ln K = \Delta G = \Delta H - T\Delta S$; the error bars indicate the uncertainty of $\pm$25%. d) Structures of truncated 21mer hairpins representing fold A and B and exchange rates between base pair imino protons and water at 293 K, as determined from the set of ^{15}N-labeled 34mer RNA sequences from Figure 2.

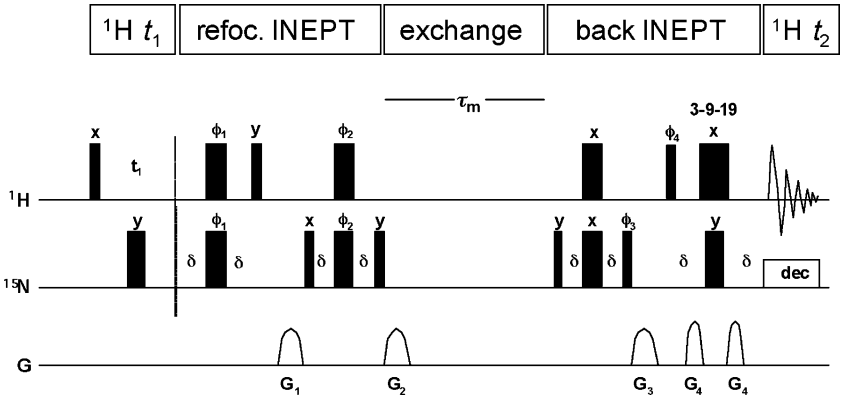

Figure 4. 2D Exchange-sensitive ^{1}H-detected ^{15}N EXSY pulse sequence used for Figure 5. In the corresponding 1D version (used for quantitative exchange studies in Figure 6), the initial proton evolution period was substituted by a selective excitation of an isolated imino proton.

inversion of the water signal[16] and 4τ was 22 ms $\approx 2/J_{NH}$. In agreement with their relative stability, the temperature dependence was much more pronounced for the G17:U4 than for the G17:C32 base pair (Figure 3b).

From the resulting relative concentrations of folds A and B, the temperature-dependent equilibrium constants $K =$ [fold A]/[fold B] were calculated. We estimated the systematic error in signal attenuation to $\pm$ 10%, resulting in an uncertainty of the equilibrium constants K of $\pm$ 25%. They ranged between $K \approx 2.4$ at 303 K and $K \approx 0.8$ at 289 K, resulting in ΔG values between $+0.1$ and -0.5 kcal mol^{-1} at 303 and 289 K, respectively (Figure 3c).

A plot of these temperature-dependent ΔG values for the transformation B $\rightarrow$ A according to the Gibbs−Helmholtz approximation (assuming temperature-independent ΔH and ΔS values) gave an estimate of the difference in enthalpies for the two coexisting folds A and B of $\Delta H = -14 \pm 3$ kcal mol^{-1}. The two truncated 21mer RNA hairpins (for structures see Figure 3d), which were designed to be representative of folds A and B, respectively, exhibit a similar relative stability $\Delta H_{truncA} - \Delta H_{truncB} = -10$ kcal mol^{-1}, as derived from the difference of enthalpies of hairpin formation determined by UV spectroscopy for the truncated fold A ($\Delta H_{truncA} = -66$ kcal/mol) and the truncated fold B ($\Delta H_{truncB} = -56$ kcal/mol), respectively (Figure 3a).

Additional experiments with ^{15}N-labeled 34mer RNA sequences were carried out to investigate the influence of the global dynamics on the local dynamics of individual base pairs. These local dynamics are reflected in the exchange rates of the corresponding imino protons with water, which were determined by selective inversion of the water signal.[16] To isolate the relevant structure-related dynamics from other contributions, we compared the water exchange rates of the 34mer RNA sequence

(16) Guéron, M.; Leroy, J.-L. *Methods Enzym.* **1995**, *261*, 383−413.

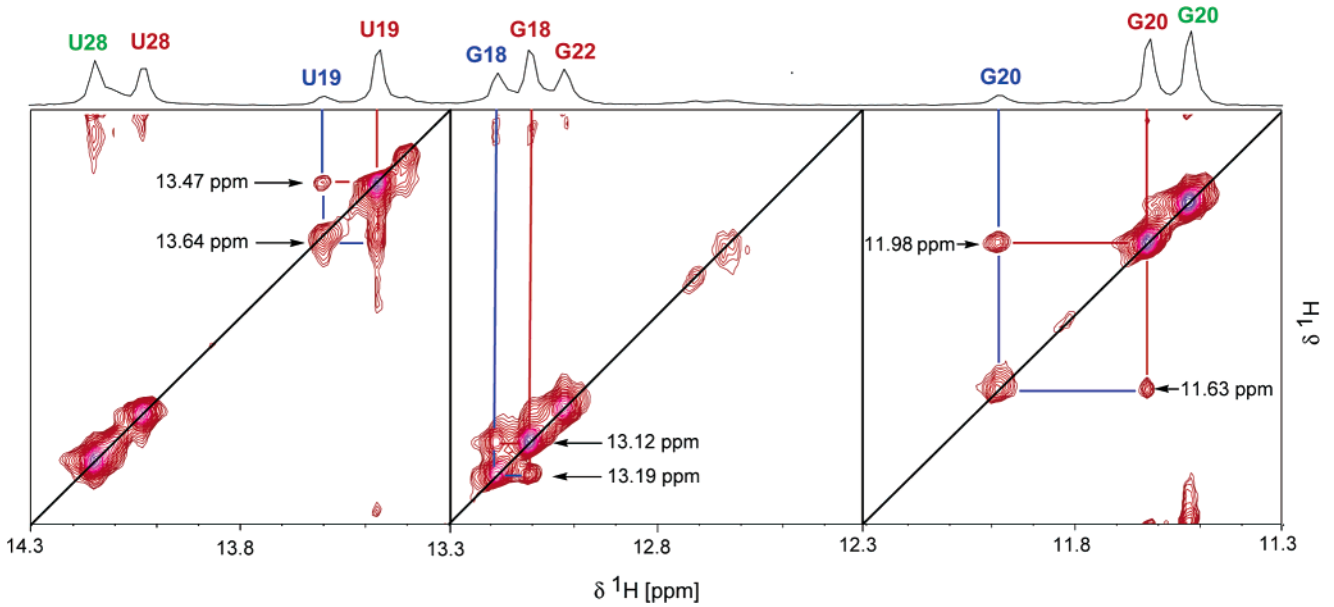

Figure 5. 2D ^{1}H-detected ^{15}N EXSY spectrum of the 34mer RNA sequence (0.8 mM, ^{15}N-labeling pattern shown in Figure 2a, the red, blue and green colors stand for folds A, B, and C respectively, as in Figure 2.), recorded with a mixing time τ_m = 400 ms at 293 K with a spectral bandwidth of 1 ppm in the vertical ω_1 domain, resulting in backfolding as indicated. The three pairs of intense cross-peaks from U19, G18 and G20 indicate that the conformational exchange rate $k_{ex,AB} = k_{A\rightarrow B} + k_{B\rightarrow A}$ between folds A and B must be > 1 s^{-1}; furthermore, the absence of detectable cross-peaks between G20 and U28 of fold C indicates its much slower conformational exchange with folds A and B with $k_{ex,AC}$ and $k_{ex,BC}$ < 0.1 s^{-1}.

with those of the two truncated 21mer RNA hairpins, representative of folds A and B. Within experimental error these rates were all identical (Figure 3d), indicating that the two folds A and B of the 34mer RNA sequence exhibit the same local base-pair dynamics as the two corresponding folds of the static truncated 21mer hairpins. This result suggests that the 34mer RNA sequence consists of a superposition of well-separated folds A and B.

2.3. Refolding Kinetics. By conventional ^{1}H EXSY spectroscopy involving imino protons, the conformational exchange between the different hairpin folds could not be analyzed. This result was not surprising and was attributed to the fast relaxation and water exchange of imino protons. Therefore, we have developed new pulse sequences where the magnetization is transferred to ^{15}N nuclei prior to the mixing period. The longitudinal relaxation times $T_1\{^{15}N\}$ are about an order of magnitude longer than $T_1\{^1H\}$ and the exchange of longitudinal ^{15}N magnetization during the mixing period is not affected by interference of water exchange competing with conformational exchange. Similar concepts have been reported by Orekhov et al.[18] and by Farrow et al.[19] for the study of slow conformational exchange in proteins and by Ferrage et al.[20] for the quantification of slow diffusion of proteins and nucleic acids.

We designed a two-dimensional exchange-sensitive ^{1}H-detected ^{15}N EXSY experiment, which shows cross-peaks between ^{15}N-bound imino protons in two different folds, if the structural exchange occurs within the time frame of ^{15}N-longitudinal relaxation. For RNA, such a ^{1}H/^{1}H correlation is preferred over a ^{1}H/^{15}N or a (hypothetical) ^{15}N/^{15}N correlation, since the chemical shift dispersion of ^{1}H signals from different RNA folds is considerably larger than that of the corresponding ^{15}N signals (see Figure 2). The new exchange-sensitive pulse sequences (Figure 4) are related to ^{15}N inversion recovery experiments, employed for the determination of ^{15}N relaxation rates. After a proton evolution period t_1, the longitudinal imino proton magnetization H_Z^A of fold A is converted into longitudinal magnetization $-N_Z^A$ of the scalar-coupled ^{15}N nuclei by a refocused INEPT sequence. If the RNA sequence undergoes a conformational exchange A → B in the subsequent time-interval τ_m, which may be on the order of $T_1\{^{15}N\}$, $-N_Z^A$ will be transferred to $-N_Z^B$ of the other fold B. After transforming $-N_Z^B$ into H_X^B, proton signals at the chemical shifts of fold B will appear in an ω_2 domain. The native N_Z-magnetization is canceled by a suitable phase cycle.

Application of this exchange-sensitive pulse sequence to a partially ^{15}N-labeled 34mer RNA sequence (see Figure 2a) resulted in the 2D ^{1}H-detected ^{15}N EXSY spectrum shown in Figure 5. Several intense cross-peaks of imino proton signals (G18, U19 and G20) were detected for the conformational exchange between folds A and B, indicating that the corresponding exchange rate $k_{ex,AB}$ (= $k_{A\rightarrow B} + k_{B\rightarrow A}$) is larger than 1 s^{-1}. In contrast, no such cross-peaks for conformational exchange involving fold C were detected and hence, the exchange between the structurally very similar folds A and B with the extended hairpin fold C must be considerably slower than the $R_1\{^{15}N\}$ relaxation rate of 1−2 s^{-1}. By comparing the noise level with simulated signal intensities (calculated by means of the Bloch−McConnell equation,[21] according to Supporting Information) a more precise estimate for the upper limit of $k_{ex,AC}$ and $k_{ex,BC}$ < 0.1 s^{-1} was obtained.

(17) Marky, L. A.; Breslauer, K. J. *Biopolymers* **1987**, *26*, 1601−1620.
(18) Orekhov, V. Y.; Korzhnev, D. M.; Pervushin, K. V.; Hoffmann, E.; Arseniev, A. S. *J. Biomol. Struct. Dyn.* **1999**, *17*, 157−174.
(19) (a) Farrow, N. A.; Zhang, O.; Forman-Kay, J. D.; Kay, L. E. *J. Biomol. NMR* **1994**, *4*, 727−734; (b) Farrow, N. A.; Zhang, O.; Forman-Kay, J. D.; Kay, L. E. *Biochemistry* **1995**, *34*, 868−878.
(20) Ferrage, F.; Zoonens, M.; Warschawski, D. E.; Popot, J. L.; Bodenhausen, G. *J. Am. Chem. Soc.* **2003**, *125*, 2541−2545.
(21) (a) Bloch, F. *Phys. Rev.* **1946**, *70*, 460−474. (b) McConnell, H. M. *J. Chem. Phys.* **1958**, *28* 430−431.

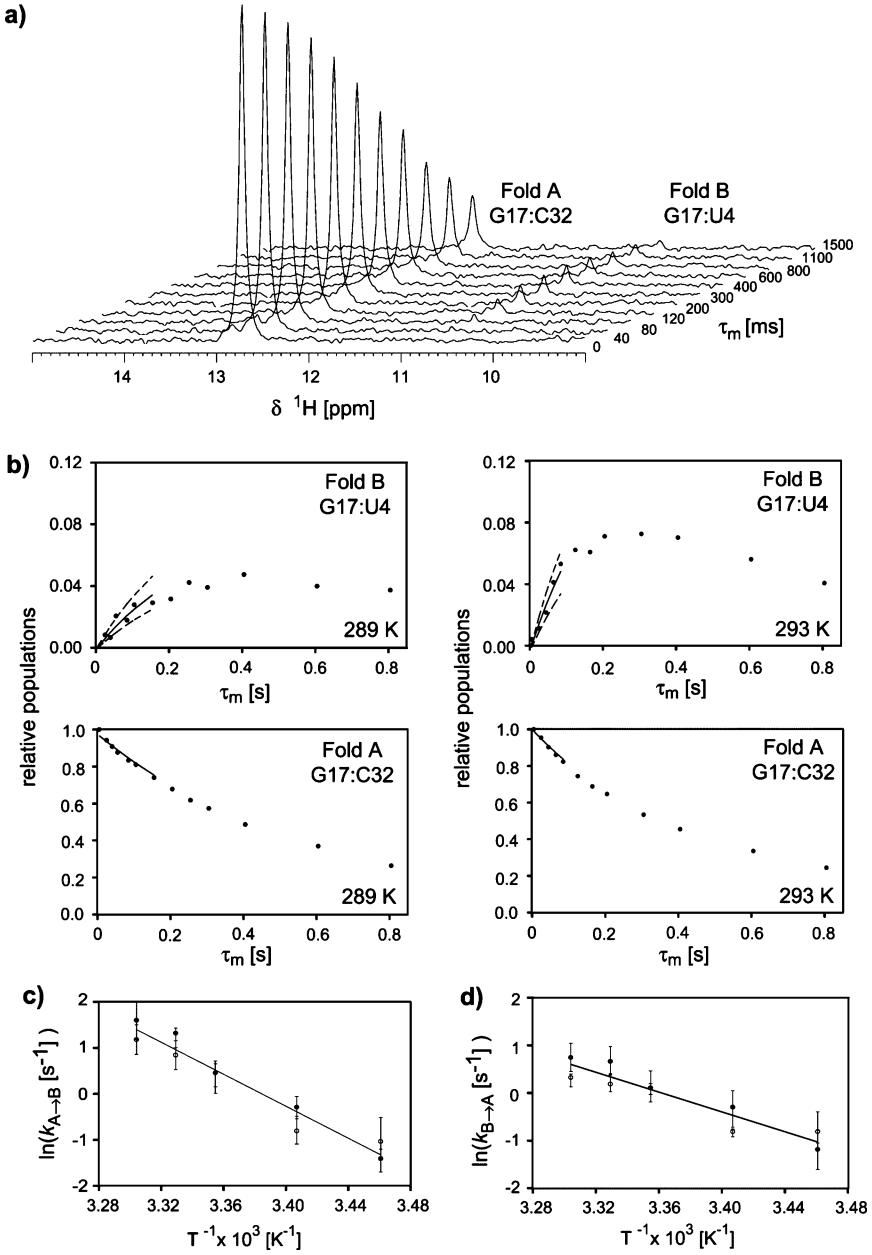

Figure 6. (a) Series of 1D ^{1}H-detected ^{15}N EXSY spectra of the ^{15N}G17-labeled 34mer RNA sequence (0.5 mM) recorded at 293 K as a function of the mixing time τ_m, after selective inversion of the G17:C32 imino proton signal at 12.8 ppm (fold A), showing the buildup of the G17:U4 signal (fold B) at 10.8 ppm as a result of conformational exchange. (b) Buildup of the G17:U4 signal (top) and decay of the G17:C32 signal (bottom) as a function of the mixing time, at 289 K (left) and 293 K (right); the initial rate curves fitted according to the Bloch−McConnell equation[21] are drawn as solid lines and the confidence interval is indicated by dotted lines. Fits obtained from excitation of the G17:U4 signal and at other temperatures are shown in the Supporting Information Figure S3. (c,d) *Arrhenius* plots of temperature-dependent rate constants $k_{A\rightarrow B}$ and $k_{B\rightarrow A}$ according to $\ln k = -E_a/(RT) + \ln A$, closed and open circles indicate values obtained from selective inversion of the imino proton signals of base pairs G17:C32 (fold A) and G17:U4 (fold B), respectively; corrected for the effects of exchange with bulk water; the error bars include the K uncertainty of ±25% and the confidence interval of the initial rate fits; detailed values are given in Supporting Information Figure S4.

To determine the refolding kinetics of the observable transition between folds A and B, a more sensitive 1D version of the ^{1}H-detected ^{15}N EXSY experiment was used, which allowed the selective excitation of either of the two well-separated imino proton resonances of the ^{15N}G17-labeled RNA sequence from Figure 1b. The required 1D pulse program was obtained by replacing the initial proton evolution period of the 2D ^{1}H-detected ^{15}N EXSY experiment (Figure 4) by a selective proton excitation. At each temperature (289, 293, 298, 300, and 303 K), two separate sets of experiments were carried out, with selective excitation of the ^{15N}G17:C32 imino proton of fold A (δ = 12.5 ppm) and of the ^{15N}G17:U4 imino proton of fold B (δ = 10.5 ppm). Each set consisted of 15 experiments with different mixing times τ_m ranging from 3 μs to 1.5 s. Figure 6a shows some traces of the experiments carried out at 293 K with selective excitation of the G17:C32 imino proton in fold A. The intensity of the G17:C32 imino proton signal decreases with increasing mixing time, mainly due to $T_1\{^{15}N\}$ relaxation and partially due to conformational exchange. The latter results in a magnetization transfer to G17:U4 in fold B and is detected as a signal at the corresponding imino proton frequency. This signal increases with mixing time due to transfer of magnetization,

but its increase is attenuated by $T_1\{^{15}N\}$ relaxation and by back-transfer. As a result, the signal buildup culminates at a transient maximum.

The intensities of the selectively excited signal and of the exchange-induced signal were translated into populations by accounting for water exchange during the INEPT steps, and plotted as a function of the mixing time. The resulting traces were fitted simultaneously to the two-state Bloch−McConnell equations[21] (see Supporting Information). As an example, four such traces obtained at 298 and 293 K are shown in Figure 6b. As fit parameters, the exchange rates $k_{ex} = k_{A\rightarrow B} + k_{B\rightarrow A}$ and the initial intensities of all signals were employed. The required $R_1\{^{15}N\}$ relaxation rates (between 1 and 2 s^{-1}, depending on the temperature) were obtained from standard longitudinal ^{15}N relaxation experiments and the equilibrium populations were obtained from the equilibrium constants K (see Figure 3c). While the inversion recovery is always dominated by R_1, the initial, quasi monoexponential part of the signal buildup depends predominantly on the relevant exchange rate k_{ex}. The initial intensities were treated as independent fitting parameters to account for potential imperfect selectivity of the excitation and for exchange during the preparation period before the mixing time τ_m. At low temperatures (289 and 293 K), reasonable fits were obtained for the whole range of mixing times, whereas at higher temperatures (298, 300, and 303 K) a significant deviation from the model was observed beyond the initial rate regime. Most probably, this is a consequence of perturbing effects at longer mixing times (e.g., heteronuclear NOEs, spin diffusion, cross-relaxation), as often observed in quantitative NOESY[22] and water exchange experiments.[16,23] Therefore, fits were carried out according to an initial rate approximation, taking into account only the first part of the buildup and inversion recovery curves. For the determination of the confidence interval, additional fits allowing for the K uncertainties were carried out and the resulting k_{ex} rates were manually varied to such an extent that the corresponding curves comprised all data points within the fitted regions (Figure 6b, Supporting Information Figure S3a,b).

To assess the worst possible interference from fold C on the apparent rate of the A → B transition at 293 K, a numerical computation of an extended three-state Bloch−McConnell equation was carried out with an estimated population of 35% fold C and an upper limit of the $k_{ex,AC}$ and $k_{ex,BC}$ values of 0.1 s^{-1} (see above). According to this simulation, the exchange with fold C contributes less than 1% to the buildup of the cross-peak relating folds A and B and could therefore be neglected (for details see Supporting Information).

Fitting of the data according to the two-state Bloch−McConnell model resulted in two independently determined values for the rate constant $k_{ex} = k_{A\rightarrow B} + k_{B\rightarrow A}$ for each temperature, one from the excitation of the imino proton of G17:U4 (fold A) and the other from the excitation of the imino proton of G17:C32 (fold B). The values for the derived rate constants k from the two independent experiments differ by 20−30% (Figure 6c,d), which is within the range of their individual uncertainties. We conclude that the experimental uncertainty of the k_{ex} values is in the same range as uncertainties arising from the obviously simplified two-state Bloch−McConnell model for the description of the magnetization transfer.

The average rate constants ranged from $k_{A\rightarrow B} = 0.3 \pm 0.1$ s^{-1} at 289 K to $k_{A\rightarrow B} = 4.1 \pm 1.2$ s^{-1} at 303 K, and those for the backward reaction from $k_{B\rightarrow A} = 0.4 \pm 0.1$ s^{-1} at 289 K to $k_{B\rightarrow A} = 1.7 \pm 0.5$ s^{-1} at 303 K. The individual rate constants were fitted according to the Arrhenius approximation to yield an activation energy $E_a = 35 \pm 6$ kcal mol^{-1} and a frequency factor $A = 10^{(26 \pm 4)}$ s^{-1} for the transformation A → B, and $E_a = 20 \pm 5$ kcal mol^{-1} and $A = 10^{(15 \pm 4)}$ s^{-1} for the transformation B → A, respectively, at a 90% confidence interval (Figure 6c,d, for detailed values see Supporting Information Figure S4).

3. Discussion and Conclusions

The refolding of thermodynamically stable, representative RNA structures, involving a sequential disruption and formation of specific base pairs is usually a relatively slow process, with typical rate constants $k = 1-10^{-4}$ s^{-1} at 25 °C. Therefore, such processes have so far been studied by creating a state of nonequilibrium concentrations and by observing the relaxation toward equilibrium.[3−12] Here, we report the first study of RNA refolding in an unperturbed dynamic equilibrium, for which we developed a new $^1H/^{15}N$-heteronuclear exchange-sensitive NMR method. The 2D version allows the detection of structural changes occurring in the time range of $T_1\{^{15}N\}$ relaxation of 0.5−1 s and the corresponding 1D version allows their straightforward quantification. Since this 1D experiment is based on selective excitation of imino protons bound to ^{15}N nuclei, ^{15}N-labeled guanosines (or uridines) are required, which must form base pairs in both interconverting structures with a sufficient ^1H chemical shift separation of the corresponding imino proton signals (in our case $\Delta\delta \approx 500$ Hz). In general, such a signal separation is observed when the frequently encountered non-Watson−Crick GU base pair is involved and switching between *G*C ↔ *G*U or *U*A ↔ *U*G base pairs occurs.[24]

The selective incorporation of ^{15}N-labeled nucleotides into a 34mer RNA sequence allowed a straightforward detection and assignment of base pairs by HNN correlation experiments, from which three coexisting folds could be unambiguously deduced. All our NMR experiments were based on the observation of imino proton signals, which advantageously appear as one singlet signal for each base pair. However, since imino protons are exchanging with water, their signal intensity is strongly affected by the opening and closing rates of the base pairs. In general, the first two or three base pairs at the ends of stems and AU/GU base pairs are less rigid than central base pairs or GC base pairs. We have employed independent experiments to measure water-exchange rates, to account for such differences in signal attenuation.

The refolding rates for the 34mer RNA sequence investigated here are approximately 40 times higher than the previously reported rates for related, thermodynamically comparable bistable 20mer RNA sequences.[12] Very likely, this difference in rates is a consequence of a different folding topology. In the previously investigated 20mer RNA sequences, all base pair contacts are affected by the refolding process, during which loop regions are converted into stem regions and vice versa. In

(22) Wüthrich, K. in *NMR of Proteins and Nucleic Acids*; John Wiley & Sons: New York, 1986.
(23) Hwang, T.-L.; van Zijl, P. C. M.; Mori, S. *J. Biomol. NMR* **1998**, *11*, 222−226.
(24) McDowell, J.; He, L.; Chen, X.; Turner, D. H. *Biochemistry* **1997**, *36*, 8030−8038.

contrast, the 34mer RNA sequence presented here contains two independent GCGA tetraloop motives, which flank the common target strand. These preorganized loops, which are both retained during refolding, nucleate the hairpin formation. This topological feature leads to an entropically favorable preorientation of the replacing strand.

The Arrhenius analysis of the temperature-dependent refolding rates revealed activation energies $E_{a,A\rightarrow B} = 35 \pm 6$ kcal mol^{-1} and $E_{a,B\rightarrow A} = 20 \pm 5$ kcal mol^{-1}, which correspond to approximately half of the total base pair enthalpy determined for the two truncated reference hairpins (ΔH of hairpin formation $= -66$ and -56 kcal/mol for the truncated forms of folds A and B, respectively). These relatively high activation energies suggest that refolding does not occur through a step-by-step zipper mechanism, but rather by a two-state process, in which the dissociation of several base pairs of one fold has to precede the formation of the base pairs of the alternative fold. This dissociative mechanism is strongly supported by the results of water exchange experiments, which revealed that the base pair dynamics of the refolding 34mer RNA sequence and the two static truncated reference hairpin sequences are identical. This indicates that the hairpin substructures in folds A and B are structurally isolated from each other and that their initial dissociation is not assisted by the unpaired, replacing strand. A step-by-step zipper mechanism, in contrast, would imply an ensemble of many intermediary structures, resulting in a highly dynamic system, in which the water exchange rates should be significantly larger than in the static reference hairpins.

In the design of the 34mer RNA sequence, the different base pair stabilities of folds A and B (containing a G17:C32 and a G17:U4 base pair, respectively) were compensated by a favorable 3′-dangling adenosine in fold B. As a consequence, the 3′-terminal base pairs of fold A are much more dynamic than the corresponding base pairs of fold B, as indicated by water exchange studies (Figure 3d) and HNN correlation experiments (Figure 2). In our opinion, this difference in dynamics is reflected in the difference of the *Arrhenius* frequency factors, which are $A = 10^{(26 \pm 4)}$ s^{-1} and $A = 10^{(15 \pm 4)}$ s^{-1} for the transformations A → B and B → A, respectively. The more labile 3′-terminal base pairs of fold A could allow a more favorable interaction (higher collision cross-section, hence a higher *A* factor) between the replacing RNA strand and the common target strand.

Very likely, the refolding of the 34mer RNA sequence investigated here occurs at an upper rate limit of systems with similar thermodynamical stability (eight base pairs, $\Delta H = 55-65$ kcal mol^{-1}). The process is entropically favored by the specific topology of this RNA sequence, which is characterized by two independent tetraloops acting as preformed nucleation sites for refolding. However, this favorable topology does not affect the refolding mechanism. The activation barriers are still relatively high and correlate approximately with the dissociation of half of the base pairs, as found for the refolding of previously reported, topologically different 20mer RNA sequences.[12]

It has been observed that structural rearrangements of RNA sequences occur considerably faster in vivo than in solution and it has been speculated that nonspecific interactions with RNA-binding proteins[25] and specific interactions with RNA-chaperons[26] are catalyzing these processes. The 1D and 2D exchange sensitive NMR methods presented here allow detection and quantification of RNA refolding processes occurring with $\tau = 1-10$ s ($k = 0.1-1$ s^{-1}) and could therefore be used for the detailed kinetic characterization of protein-catalyzed RNA refolding.

4. Experimental Section

4.1. Preparation of RNA Sequences. The assembly of all RNA sequences was carried out under standard conditions[27] in a 1.0 μmol-scale on a Gene Assembler (*Pharmacia*) from 2′-*O*-TOM protected phosphoramidites and the corresponding solid supports; the synthesis of the standard and the ^{15}N-labeled phosphoramidites is reported elsewhere.[14,27] After standard deprotection, all RNA sequences were purified by anion exchange HPLC, isolated as triethylammonium salts and analyzed by LC−ESI or MALDI-ToF−MS as described previously.[14]

r[CACUUGAGGCGACUCA(^{15}N)GUGAGGCGACUCACCUG] (Figure 1a,b, 5a, Supporting Information Figure S2): *m/z* 10930 (calcd.: 10930); r[CACUUGAGGCGACUCAG(^{15}N)(^{15}N)(^{15}N)-(^{15}N)(^{15}N)GCGA(^{15}N)(^{15}N) (^{15}N)(^{15}N)(^{15}N)CUG] (Figure 2a): *m/z* 10939 (calcd.: 10939); r[CACUUGAGGCGACU(^{15}N)(^{15}N) (^{15}N)GUGAGGCGACUCAC(^{15}N)(^{15}N)(^{15}N)] (Figure 2b): *m/z* 10935 (calcd.: 10935); r[CACU(^{15}N)(^{15}N)(^{15}N)(^{15}N)GCGA(^{15}N)-(^{15}N)(^{15}N)(^{15}N)GGUGAGGCGACUCACCUG] (Figure 2c): *m/z* 10935 (calcd.: 10937); r[(^{15}N)(^{15}N)(^{15}N)UUGAGGCGACUCAG-(^{15}N)(^{15}N)(^{15}N)AGGCGA CUCACCUG] (Figure 2d, 4, Supporting Information Figure S2): *m/z* 10935 (calcd.: 10935); r[CACUU(^{15}N)G)-AGGC(^{15}N)AC(^{15}N)CAGGUG(^{15}N)A)GG(^{15}N)C)GACU(^{15}N)C) AC-CUG] (Figure 2e): *m/z* 10937 (calcd.: 10935); r[CACUUG(^{15}N)A)-(^{15}N)GCGA(^{15}N)C)U(^{15}N)C)AGGU(^{15}N)G)A(^{15}N)G)GCGA(^{15}N)C) (^{15}N)U)CAC-CUG] (Figure 2f): *m/z* 10937 (calcd.: 10937); r[CACUUGAGGCGA-CUC(^{15}N)A)GG(^{15}N)U)GAG GCGACUCACCUG] (Supp. Fig. S1): *m/z* 10932 (calcd.: 10931); r[CACUUGAGGCGACUCA GGUG(^{15}N)A)GGC-GACUCACCUG] (Supporting Information Figure S1): *m/z* 10931 (calcd.: 10930); r[CACUUGAGG CGAC(^{15}N)U)CAGGUGAGGCGA-CUCACCUG] (Supporting Information Figure S1): *m/z* 10931 (calcd.: 10930); r[CACUUGAGGCGACUCAGGUGA] (Figure 3): *m/z* 6751 (calcd.: 6751). r[UCAGGUGAGGCG ACUCACCUG] (Figure 3): *m/z* 6728 (calcd.: 6727).

4.2. Thermal Denaturation Studies in Figure 3a. The UV absorbance was recorded as a function of temperature at 260 nm on a Cary Bio-1 spectrophotometer (Varian) equipped with a Peltier temperature controlling device. The samples were dissolved in aqueous potassium arsenate buffer (25 mM, pH 7.0). Prior to the measurements, each sample was briefly heated to 80 °C. The curves were obtained with cooling and heating ramps of 0.5 °C min^{-1} and translated into hyperchromicity (Figure 3a) or α versus T^{-1} plots. From the latter the ΔH values of hairpin formation were determined according Marky and Beslauer.[17]

4.3. NMR Experiments−General. NMR experiments were carried out on a AV 600 MHz spectrometer (*Bruker*) equipped with a 5 mm TXI−HCN cryogenic probe with z-gradients. The RNA samples (amounts determined spectrophotometrically) were dissolved in 0.3 mL potassium arsenate buffer (25 mM, pH 7.0) in H_2O/D_2O (9:1). Restricted volume *Shigemi* tubes were used for all experiments. Spectra were processed with XWINNMR and plotted with XWINPLOT.

4.4. 1D NMR Experiments in Figure 1, Figure 2, and Supporting Information Figure S1 and S2. 1D ^{1}H spectra were recorded by combining a water flip-back pulse and 3-9-19 WATERGATE for suppression of the water signal. ^{15}N-filtered ^{1}H spectra were recorded

(25) Schroeder, R.; Grossberger, R.; Pichler, A.; Waldsich, C. *Curr. Opin. Struct. Biol.* **2002**, *12*, 296−300.

(26) Herschlag, D. *J. Biol. Chem.* **1995**, *270*, 20871−20874.

(27) Pitsch, S.; Weiss, P. A.; Jenny, L.; Stutz, A. Wu, X. *Helv. Chim. Acta* **2001**, *84*, 3773−3795.

with an HSQC sequence with $t_1 = 0$ and a refocused INEPT transfer as ^{15}N filter, and 3-9-19 WATERGATE for suppression of the water signal.

4.5. Water Exchange NMR Experiments in Figure 3b and d. Water exchange rates in Figure 3b and d were determined with the RNA sequence shown in Figure 1 and with the set of four ^{15}N-labeled 34mer RNA sequences shown in Figure 2a−d, respectively; water exchange rates in Figure 3b and d were extracted from ^{15}N-filtered ^{1}H experiments by selective inversion of the water signal according to Guéron and Leroy.[16]

4.6. Determination of the Equilibrium Constants *K* in Figure 3c. The temperature-dependent equilibrium constants $K = [A]/[B]$ (= [fold A]/[fold B]) were calculated from the intensities of G17:C32 and G17:U4 imino proton signals derived from the ^{15}N-filtered ^{1}H spectra of the ^{15N}G17-labeled RNA sequence at 289, 293, 298, 300, and 303 K (see Supporting Information Figure S2). After integration by Lorentzian fitting, the integrated signal intensities (I) were transformed into relative concentrations (c_{rel}) according to $c_{rel} = I/\exp\{-4\tau\ k_{H2O}\}$; with k_{H2O} (water exchange rates): obtained from the separate experiments in Figure 3b, and with 4τ (duration of the forward and backward refocused INEPT steps): 22 ms. From the K values, the thermodynamic parameters ΔG and ΔH were determined by linearization according to Gibbs−Helmholtz ($-RT \ln K = \Delta G = \Delta H - T\Delta S$, Figure 3c). The uncertainty of the K values was estimated to be ±25%.

4.7. 2D ^{1}H-Detected ^{15}N EXSY Experiment in Figure 5. The pulse sequence is shown in Figure 4; the spectrum was recorded with a mixing time $\tau_m = 400$ ms, 400 transients, a spectral width of 1 ppm (centered at the carrier frequency at 12.8 ppm) and 64 time increments in the indirect dimension.

4.8. 1D ^{1}H-Detected ^{15}N EXSY Experiments in Figure 6 and Supporting Information Figure S3. Two sets of experiments were carried out, one with selective inversion (Gaussian, 4.7 ms) of the G17:C32 imino proton and the other with selective inversion of the G17:U4 imino proton. For each set, exchange experiments were carried out at 289, 293, 298, 300, and 303 K by recording a series of spectra at each temperature with different mixing times (up to 2000 ms, as indicated in Figure 6 and Supporting Information S3) and 1024 transients at 289 and 293 K or 512 transients at 298, 300, and 303 K.

4.9. Kinetic Experiments in Figure 6 and Supporting Information S3 and S4−Data Collection and Analysis. For the determination of the refolding rates by the 1D ^{1}H-detected ^{15}N EXSY experiment, the imino proton signal intensities for the ^{15}N-labeled base pairs G17:C32 and G17:U4 were obtained by Lorentzian-fitting and corrected for different water exchange rates. The 'diagonal' signal I_{AA} resulting from selective excitation in fold A was corrected according to $I_{AA}^{corr} = I_{AA}/\exp\{-4\tau\ k_{H2O,A}\}$, whereas the 'cross-peak' signal I_{AB} resulting from exchange after selective excitation in fold A was corrected according to $I_{AB}^{corr} = I_{AB}/\exp\{-2\tau(k_{H2O,A} + k_{H2O,B})\}$. Corresponding formulas were applied to obtain I_{BB}^{corr} and I_{BA}^{corr}. For the determination of water exchange rates k_{H2O}, see Experimental 4.5; 4τ and 2τ were 22 and 11 ms, respectively.

The first part of the buildup curves (water exchange-corrected intensities of the detected signal as a function of the mixing time, see Figure 6b and Supporting Information Figure S3) were fitted by an initial rate approximation to the solution of the two-state Bloch−McConnell equations,[21] as summed up in the Supporting Information. From the temperature-dependent equilibrium constant K (see Experimental 4.6), the relative populations p_A and p_B were calculated and the parameters $k_{A\to B} = p_B\ k_{ex}$ and $k_{B\to A} = p_A\ k_{ex}$ were reduced to the exchange rate $k_{ex} = k_{A\to B} + k_{B\to A}$. The exchange rate k_{ex} and the initial intensities at $t = 0$ were treated as independent fitting parameters, allowing the buildup to start at values different from zero. This accounts both for possible imperfect selectivity and for exchange that may occur during the preparation. The rate constants $k_{A\to B}$ were obtained from $k_{A\to B} = k_{ex}/(1 + K)$. The determination of the confidence intervals (CI) of the individual rate constants was carried out as follows: First, to account for the ±25% uncertainty estimated for the K values, two other fits with $K^+ = 1.25\ K$ and $K^- = K/1.25$ were carried out. Then, to account for the variation of the data points from the buildup curves, the k_{ex} values were varied manually to such an extent that the resulting curve fits for k_{ex}^+ and k_{ex}^- visually comprised all data points within the fitted region. The CI of the $k_{A\to B}$ values was then estimated by setting the upper limit to $k^+_{A\to B} = k_{ex}^+/(1 + K^+)$ and the lower limit to $k^-_{A\to B} = k_{ex}^-/(1 + K^-)$. The $k_{B\to A}$ values were obtained from $k_{B\to A} = k_{ex}\ K\ /\ (1 + K)$. The CI of the $k_{B\to A}$ values were then estimated by setting the upper limit to $k^+_{B\to A} = [k_{ex}^+\ K^+\ /\ (1 + K^+)]$ and the lower limit to $k^-_{B\to A} = [k_{ex}^-\ K^-\ /\ (1 + K^-)]$. All fits and k_{ex} values are shown in Supporting Information Figure S3 and all derived rate constants k are shown in the Supporting Information Figure S4. The kinetic parameters E_a and A for the forward and backward reactions were determined by linearization from all $k_{A\to B}$ and $k_{B\to A}$ values, respectively, as shown in Figure 6c,d. The 90% confidence intervals for E_a and A values were obtained from the standard deviation of the linear regression multiplied by the appropriate Student-t factor.

Acknowledgment. The work was supported by the EPFL, the Swiss National Science Foundation, the Commission for Technology and Innovation (KTI), and Carlsbergfondet. NMR experiments were performed at the Suisse Romande high field spectrometer facility (EPF Lausanne) and the inSPIN spectrometer facility (Aarhus Universitet).

Supporting Information Available: Additional HNN correlation experiments for duplex/hairpin discrimination, temperature-dependent ^{15}N filtered ^{1}H spectra, all fits of exchange-sensitive 1D experiments, k_{ex} and k values are summarized in Figures S1-S4; the Bloch−McConnell equations and their solutions are also given. This material is available free of charge via the Internet at http://pubs.acs.org.

JA060344A